Sputter deposition of porous thin films from metal/NaCl powder targets EP

R. Dedoncker, H. Rijckaert iD, and D. Depla

COLLECTIONS

EP This paper was selected as an Editor's Pick

View Online   Export Citation   CrossMark

ARTICLES YOU MAY BE INTERESTED IN

Net negative fixed interface charge for Si_3N_4 and SiO_2 grown in situ on 000-1 N-polar GaN
Applied Physics Letters **115**, 032103 (2019); https://doi.org/10.1063/1.5111148

Hole-doped M_4SiTe_4 (M=Ta, Nb) as an efficient p-type thermoelectric material for low-temperature applications
Applied Physics Letters **115**, 043901 (2019); https://doi.org/10.1063/1.5109590

In-phase supermode operation in GaN-based vertical-cavity surface-emitting laser
Applied Physics Letters **115**, 041101 (2019); https://doi.org/10.1063/1.5104289

Sputter deposition of porous thin films from metal/NaCl powder targets (EP)

R. Dedoncker,[1,a)] H. Rijckaert,[2] (iD) and D. Depla[1]

AFFILIATIONS

[1]Department of Solid State Sciences, Ghent University, Krijgslaan 281 (S1), 9000 Ghent, Belgium
[2]Department of Chemistry, Ghent University, Krijgslaan 281 (S3), 9000 Ghent, Belgium

[a)]Electronic mail: Robin.Dedoncker@ugent.be

ABSTRACT

A method to deposit porous thin films is elucidated. For this purpose, NaCl powder was mixed with a metal powder, cold pressed, and used as a target material in order to deposit a metal/NaCl thin film by DC magnetron sputtering. The thin film was immersed in water after deposition to remove the salt and to obtain a porous film. The low thermal conductivity of the target results in target heating and salt sublimation. In this way, the salt content in the layer and hence the film porosity are controlled by the discharge power. This procedure was carried out for Cu and Ti. The study focuses on the deposition of porous Cu thin films. From scanning transmission electron microscopy images, two film structures were observed. Films with a density higher than ≈40% of the bulk density exhibit a homogeneous spongelike microstructure with pores around 20 nm. At lower density, a noncontinuous, fractured layer is formed. The blocks between the observed cracks manifest itself in the form of columnar pores. The lowest measured density was ≈23% of the bulk density. This approach combines the flexibility of powder targets and the scalability of magnetron sputtering and avoids the usage of aggressive chemicals.

Porous thin films have a wide application field. The main applications connect to (catalytic) chemical reactions at the surface of the porous films. The large contact area makes them ideal host materials for catalysts and/or to act as catalytic materials.[1–3] In the same context, porous thin films are present in devices such as thin film batteries,[4,5] fuel cells,[6,7] gas sensors,[8,9] thermochromic windows,[10] and dye sensitized solar cells.[11] Other applications are related to their low-k dielectric properties, low refractive index, and thermal conductivity.[12] An example of the latter is thermal barrier coatings to protect sensitive surfaces from intense heat.[13] Thin film growth can be achieved by a large number of techniques.[12] The scalability of magnetron sputter deposition is one of the major benefits of reactive magnetron sputter deposition.[14] Another characteristic feature of sputter deposition is its relatively high film density.[14] The high momentum and energy of the sputtered and reflected atoms are the underlying physical reason for film densification.[15–20] This feature of magnetron sputtering hinders its direct usage to grow porous thin films. Two groups of methods try to solve the latter problem. The first group aims to reduce the energy/momentum of the arriving species on the substrate by increasing the deposition pressure and/or the target-substrate distance.[21–23] The scattering of atoms originating from the target with working gas atoms reduces their energy. One therefore refers to this deposition regime as ballistic deposition (or the hit-and-stick regime according to the structure zone model[24]). The approach has some major disadvantages despite its simplicity. The scattering process results in a decrease in the overall deposition rate and an increase in the redeposition of the sputtered material on the target. The presence of insulating thin films on the target facilitates arcing which leads to plasma instabilities and film and target damage. A popular approach, also belonging to the first group, is glancing angle deposition (GLAD). An excellent overview of GLAD is presented by Barranco *et al.*[25] The motion of a tilted substrate in this technique can be controlled in a complex way to generate films consisting of nanosized columns with well-defined shapes such as zig-zags and spirals. The flexibility in tuning the porosity and microstructure is one of the main advantages of GLAD, but the substrate manipulation still prevents to scale GLAD for industrial applications. The second group of techniques uses the full potential of sputter deposition but treats the film to induce porosity. Electrochemical leaching or dealloying of one of the constituent elements of the film is a first example of this approach.[26] A thermal treatment of the deposited film results in the decomposition of the deposited mixture of two immiscible elements. Quite often, this leads to a specific microstructure defined by processes such as spinodal decomposition. By an electrochemical treatment, one of the elements dissolves leaving a porous

structure behind. The electrochemical treatment without an intermediate heat treatment can also directly result in a porous film. Recently, Lu *et al.* illustrated that dealloying is also possible by sublimation of one of the elements.[27] A second example within this second group is the reduction of the sputtered oxide thin film by hydrogen.[28] The chemical treatment of the oxide induces the formation of a porous metal film. The two examples illustrate that magnetron sputter deposition has many other advantages such as the easiness to tune the film composition by combining several sources or by the addition of a reactive gas to the plasma to deposit oxides and/or nitrides. However, the proposed post-treatments have some major disadvantages as they are limited by the sample size and/or depend strongly on the material choice. Moreover, some of the post-treatments proposed in the literature are based on environmentally unfriendly chemicals. In this paper, an alternative approach, belonging to the second group, is demonstrated. The approach wishes to overcome the barriers of the second group to allow the application of porous thin films on an industrial scale.

Thin films were deposited in a stainless steel vacuum chamber which was pumped by a combination of rotary and turbomolecular pumps to reach a base pressure of less than 3×10^{-4} Pa as measured with a Penning gauge (Compact Full Range gauge, Pfeiffer Vacuum). The argon flow was set to 20 sccm by a mass flow controller (MKS instruments) to obtain a pressure of 0.5 Pa. The magnetron was powered with a Hüttinger 1500 DC power supply. The target-to-substrate distance was maintained at 63 mm. The substrates were cut from (111) oriented silicon wafers, RCA cleaned prior to the deposition. On a home-made 2 in. planar cylindrical magnetron, a powder target was mounted. The sample was neither cooled nor heated during the deposition. Its temperature did not exceed 150 °C. The powder targets are produced according the following procedure.[29] Copper (Cu) (Alpha Aesar, particle size: 0.044 mm) and NaCl salt (Union Chimique Belge, particle size: 0.1 mm) were thoroughly mixed with a pestle and mortar. This mixture was uniaxially cold-pressed with a load of 1.6×10^2 kN into a 2 mm disk. For this study, two sets of targets with different NaCl contents, i.e., 5 and 10 at. %, were produced. The targets with a higher NaCl content could not be used at a high discharge current as strong arcing was observed which hinders well-controlled process conditions. The addition of NaCl to the target lowers the discharge voltage at constant current. At 0.12 A, the discharge voltage of the high content target is on average 502 V, while the discharge voltage increases to 550 V at a lower NaCl content. This behavior can be understood from the much higher ion-induced electron yield for NaCl (approximately 1.2) as compared to the value for Cu (approximately 0.1 at the same argon energy).[30] Under the given conditions, depositions at different discharge powers were performed by controlling the discharge current. The deposition rate was determined based on the deposition time and thickness, obtained from contact profilometry (Taylor-Hobson Talystep). The NaCl content in the layers was determined by energy dispersive X-ray spectroscopy (EDX), while the density was calculated from the critical angle obtained by X-ray reflectivity (XRR). For the former, a FEI Quanta 200F EDS was utilized with a beam current of 208 μA and a voltage of 20 kV. On the same device, scanning electron microscopy (SEM) was conducted for planar- and cross-sectional views. The latter views were retrieved by breaking the sample. XRR measurements were taken on a Bruker D8 Advance with a scintillation detector and Cu Kα radiation, from 0.3° up to 1° with a step size

of 0.01°. X-ray diffraction (XRD) was performed on a Bruker D8 Discover equipped with a LynxEye silicon strip detector in the Bragg-Brentano configuration with Cu Kα radiation. XRD patterns of the thin films were taken from 20° up to 100° with a resolution of 0.02° per step and a step time of 1 s. The porosity of the Cu thin films was further analyzed using the scanning transmission electron microscopy (STEM) technique via a Cs-corrected JEOL JEM 2200-FS instrument operated at 200 kV with a high angle annular dark-field (HAADF) detector. Cross-sectional view HAADF-STEM lamellae were prepared via the Focused Ion Beam (FIB) technique in a FEI Nova 600 Nanolab Dual Beam FIB SEM.[31] The lamellae were extracted using the *in situ* lift out procedure with an Omniprobe extraction needle. As the deposition rate is known, it is possible to obtain from the measured composition (EDX) and the film density (XRR) the atomic flux of both NaCl and Cu. These are shown in Fig. 1. A linear increase in the copper atomic flux is observed as a function of the discharge power. This behavior is expected for sputter deposition. To validate the trend, the experimental setup was implemented in the test particle Monte Carlo simulation package SIMTRA[32] which permits us to calculate the transfer probability of sputtered atoms. The sputter yield dependency on the discharge voltage for a copper target was taken from Boydens *et al.*[33] With this information at hand, the atomic flux at the substrate was calculated as a function of the discharge power, and good agreement between experiment and simulation is obtained (see closed square markers in Fig. 1). In contrast to the linear trend for copper, an exponential increase in the molecular NaCl flux is observed. Using the same strategy as for copper with published sputter yields for NaCl, the NaCl flux at the substrate can be calculated (see closed round markers
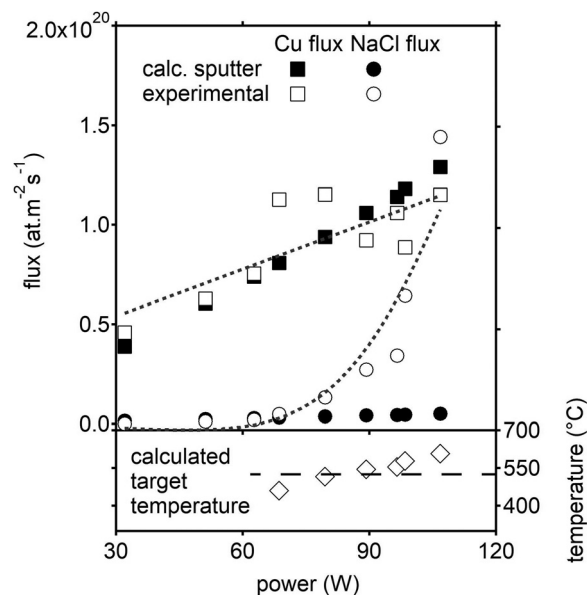

FIG. 1. The experimental (open markers) and the calculated atomic (molecular) (closed markers) flux as a function of the discharge power. Used target composition 5 at. %/95 at. %. NaCl/Cu. The calculated sputter fluxes are based on published sputter yield data and Monte Carlo simulations (see the text). The dotted lines are intended as guides to the eye. The bottom graph shows the calculated target temperature as a function of the discharge power. The dashed line indicates the Draper point at 525 °C.

in Fig. 1). A clear discrepancy with the experiment is observed. This indicates that another process besides sputtering defines the NaCl deposition flux. Based on the observation that the target glows after the experiments (see the supplementary material), it is clear that lower thermal conductivity of the target results in target heating, and hence, sublimation of the salt contributes to the molecular flux toward the sample. The target temperature can be estimated based on the following reasoning. Based on SIMTRA simulations, it is possible to calculate the transfer probability of a NaCl molecule and hence the required flux from the target. Taking into account the temperature dependency of the vapor pressure[34,35] and assuming that the target flux corresponds to the maximum sublimation rate, an estimate of the target temperature can be calculated. In this calculation, an area from which sublimation occurs is taken as $10\,cm^2$, which corresponds to the racetrack area. The following argumentation can be given for this choice. Visual inspections (see the supplementary material) show that it is mainly the racetrack area that glows after the power is switched off. Of course, the temperature outside the racetrack could be lower than the Draper point, and visual inspection is an incomplete proof. However, as the evaporation rate depends exponentially on the temperature, a lower temperature outside the racetrack means anyway a much lower contribution to the evaporation process. A second argument to take the racetrack as the sublimation area is the low thermal conductivity of the target. This is the very reason why the target becomes hot. A linear increase in the target temperature with the discharge power is found (see the lower part of Fig. 1). The dashed line in this graph indicates the Draper point,[36] the temperature at which an object emits radiation in the visible spectrum. As the depositions at the highest discharge powers showed the predicted red-glow after deposition (see also the supplementary material), the calculation of the target temperature appears accurate. Hence, the process is a combination of the sputter deposition of Cu and sublimation of NaCl from a hot target. This explains the high NaCl concentration in the film despite the low target content. Indeed, above a discharge power of 70 W, the NaCl
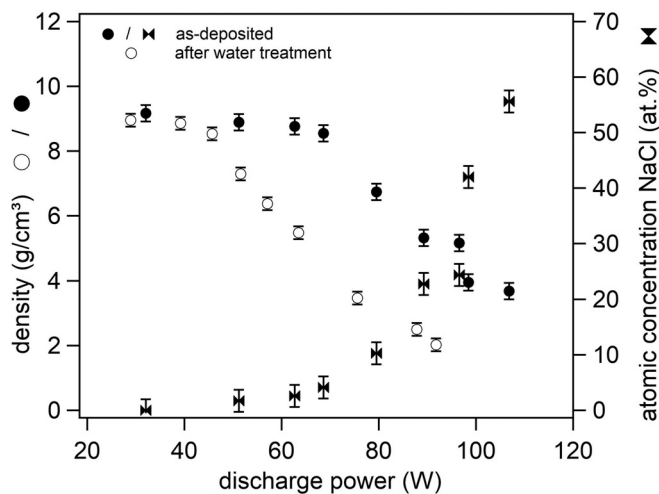
content is higher than 5 at. %. At the highest power (approximately 110 W), the salt content increases up to $\approx$56 at. % in the film. Due to the additional flux from the sublimation of NaCl, the deposition rate vastly increases with discharge power, up to 7 nm/s. A separation of both fluxes by, for example, a combination of a magnetron for the metal and an evaporation crucible for the salt would allow a higher control of the chemical composition and film thickness. On the other hand, it would also increase the complexity of the deposition setup which could be a barrier for industrial applications. Figure 2 presents, as a function of the discharge power, the film density on the left axis for two series of depositions, sputtered from a target with 5 at. % NaCl. An as-deposited series is indicated with filled markers, a series which was immersed in water immediately after deposition is represented with open markers. In the same figure, the atomic concentration NaCl of the as-deposited series is shown on the right axis. Comparison of the plotted values shows how the increase in the salt content in the thin film translates into a decrease in density. Figure 3 shows the planar view and cross sections for the thin film deposited at low and high NaCl contents. The micrographs of the as-deposited thin films (a) and (d) show the presence of NaCl crystals (white regions), partially deliquesced due to the hygroscopic nature of NaCl. The origin of these
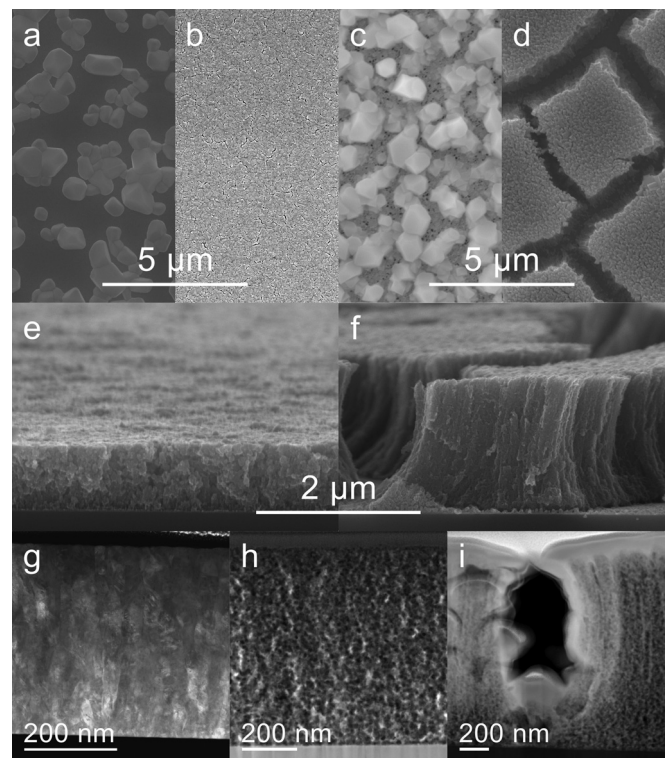

FIG. 3. SEM and TEM micrographs. The top row images are SEM top view micrographs. Middle and bottom row images are SEM and TEM micrographs in the cross-sectional view, respectively. (a), (b), and (e) show a film with a NaCl content of approximately 14 at. %, while (c), (d), and (f) show films deposited with more than 40 at. % NaCl (55 at. %, 42 at. %, and 42 at. %, respectively). (a) and (c) Before water treatment. (b)–(f) After water treatment. HAADF-STEM images on the bottom row are taken from a pure copper film (g, 29 W), spongelike microstructure (h, 63 W), and island microstructure (i, 92 W), all water-treated prior analysis.

FIG. 2. Density measurements on an as-deposited series (filled markers) and a series after water treatment (open markers). The atomic concentration NaCl of the as-deposited series is shown on the right axis. Both series were deposited from a Cu powder target with 5 at. % NaCl at an argon pressure of 0.5 Pa.

crystals is related to the deposition procedure. Due to the construction of the deposition setup, it was not possible to shield the substrate immediately after switching off the magnetron. As the target is still hot, the NaCl deposition from sublimation continues while no copper is deposited. We indeed observe that the NaCl crystals are only present on the surface and do not penetrate in the layer. As it takes approximately 10 s to remove the sample from the chamber after switching off the source, the error on the measured NaCl content induced by this artifact is of the order of a few percent. This problem can be easily overcome by the installation of a shutter. After immersion in water for a few seconds, the salt crystals clearly disappear (b) and (e), and a porous structure (c) and (f) is obtained. In the case of a high NaCl content, clear desiccation cracks can be observed. Within the remaining "islands," a similar porous structure to the low NaCl content films can be seen. The transition from a full dense copper film to a highly porous microstructure can be even better evaluated by a high angle angular dark-field transmission electron microscope (HAADF-TEM) as shown in the bottom line of Fig. 3. At low discharge current, the salt content in the film is negligible, and a pure, dense copper film (g) is observed. At higher discharge current, both the deposition rate and the salt content increase. The dark regions in Fig. 3(h) correspond to the empty spaces in the microstructure, which covers approximately 50% of the measured region. This agrees quite well with the measured porosity by XRR (40%). At even higher discharge currents (i), and hence larger salt content, large open spaces can be observed while the remainder of the film shows a similar porosity to the film deposited at intermediate discharge current. This island microstructure has a density of 23% of the bulk value according to XRR. The samples were also investigated by X-ray diffraction (not shown). Two clear Bragg reflections related to NaCl are observed before the sample has been immersed in water. These reflections disappear after the water treatment. Samples deposited at low power, i.e., low NaCl content, are pure Cu thin films. The copper reflections disappear above a discharge power of 63 W (film with 14 at. % NaCl) and are replaced by reflections which can be assigned to Cu_2O. The water treatment is not the main cause of the oxidation of the porous copper film because for films with the highest NaCl content (or discharge power), the Bragg reflections of the oxide are already present before the water treatment. The accelerated corrosion of copper in the presence of NaCl during atmospheric exposure has been described in the literature[37] and explains the presence of Cu_2O in these films. The above procedure has been repeated with titanium instead of copper. In the supplementary material, an assembled picture of snapshots from a video which captures the plasma discharge can be found. The evolution from a blue color to a yellow color can be explained from the excitation of Na-ions in the plasma when the target heats up and thus sublimation increases. Immediately after switching off the plasma, the red-glowing racetrack can be seen, indicating a temperature of more than 525 °C. The latter observation is in agreement with the results presented in Fig. 1. In addition to these snapshots, also micrographs of porous Ti films can be found. The main discrepancy with copper is that the layer remains uniform (without cracks), even at high porosities. From XRD measurements, it can be concluded that an amorphous layer forms. This indicates that the titanium metal has reacted.

In summary, a straightforward method to deposit porous thin films by magnetron sputtering has been described. Despite the simplicity of this method, further investigation is needed to investigate other salt/metal combinations and the compatibility with reactive gas addition to the discharge to permit the control deposition of porous compounds.

See the supplementary material for Figs. S1 and S2. Fig. S1 shows snapshots of a video where a target based on a mixture of Ti and NaCl is shown during and after glow discharge. The visual evolution of a blue light toward a yellow light is due to the sublimation of NaCl, and the red-afterglow is also seen after the plasma extinguishes. Fig. S2 provides an overview of SEM images from films deposited from the same Ti(NaCl) target. A complex, porous morphology can be observed.

REFERENCES

[1]T. T. N. Nguyen, Y. H. Chen, M. Y. Chen, K. B. Cheng, and J. L. He, "Multifunctional Ti-O coatings on polyethylene terephthalate fabric produced by using roll-to-roll high power impulse magnetron sputtering system," Surf. Coat. Technol. **324**, 249–256 (2017).

[2]M. Ratova, R. Klaysri, P. Praserthdam, and P. J. Kelly, "Pulsed DC magnetron sputtering deposition of crystalline photocatalytic titania coatings at elevated process pressures," Mater. Sci. Semicond. Process. **71**, 188–196 (2017).

[3]H. Wang, G. D. Shi, X. S. Zhang, W. Zhang, L. Huang, and Y. Yu, "In-situ synthesis of TiO_2 rutile/anatase heterostructure by DC magnetron sputtering at room temperature and thickness effect of outermost rutile layer on photocatalysis," J. Environ. Sci. **60**, 33–42 (2017).

[4]M. T. Demirkan, L. Trahey, and T. Karabacak, "Low-density silicon thin films for lithium-ion battery anodes," Thin Solid Films **600**, 126–130 (2016).

[5]M. C. Thirumoolam, B. Sivaramakrishnan, and M. Devarajan, "Sputtering deposition of aluminium molybdenum alloy thin film anodes for thin film microbatteries," Electron. Mater. Lett. **11**, 416–423 (2015).

[6]J. Fondard, A. Billard, G. Bertrand, S. Fourcade, P. Batocchi, F. Mauvy, and P. Briois, "Effect of total pressure on La_2NiO_4 coatings deposited by reactive magnetron sputtering using plasma emission monitoring," Surf. Coat. Technol. **295**, 29–36 (2016).

[7]F. J. Garcia-Garcia, F. Yubero, A. R. Gonzalez-Elipe, and R. M. Lambert, "Microstructural engineering and use of efficient poison resistant Au-doped Ni-GDC ultrathin anodes in methane-fed solid oxide fuel cells," Int. J. Hydrogen Energy **43**, 885–893 (2018).

[8]D. Abubakar, N. M. Ahmed, S. Mahmud, and N. A. Algadri, "Properties of NiO nanostructured growth using thermal dry oxidation of nickel metal thin film for hydrogen gas sensing at room temperature," Mater. Res. Express **4**, 075009 (2017).

[9]Q. A. Drmosh, Z. H. Yamani, and M. K. Hossain, "Hydrogen gas sensing performance of low partial oxygen-mediated nanostructured zinc oxide thin film," Sens. Actuators, B **248**, 868–877 (2017).

[10]S. Bogati, A. Georg, and W. Graf, "Photoelectrochromic devices based on sputtered WO_3 and TiO_2 films," Sol. Energy Mater. Sol. Cells **163**, 170–177 (2017).

[11]S. Sanzaro, E. Fazio, F. Neri, E. Smecca, C. Bongiorno, G. Mannino, R. A. Puglisi, A. La Magna, and A. Alberti, "Pervasive infiltration and multi-branch chemisorption of N-719 molecules into newly designed spongy TiO_2 layers deposited by gig-lox sputtering processes," J. Mater. Chem. A **5**, 25529–25538 (2017).

[12]P. Kumar, K.-H. Kim, K. Vellingiri, P. Samaddar, P. Kumar, A. Deep, and N. Kumar, "Hybrid porous thin films: Opportunities and challenges for sensing applications," Biosens. Bioelectron. **104**, 120–137 (2018).

[13]K. D. Harris, D. Vick, E. J. Gonzalez, T. Smy, K. Robbie, and M. J. Brett, "Porous thin films for thermal barrier coatings," Surf. Coat. Technol. **138**, 185–191 (2001).

[14]D. Depla, S. Mahieu, and J. E. Greene, "Chapter 5: Sputter deposition processes A2," in *Handbook of Deposition Technologies for Films and Coatings*, 3rd ed., edited by Peter M. Martin (William Andrew Publishing, Boston, 2010), pp. 253–296.

[15]D. W. Hoffman, "A sputtering wind," J. Vac. Sci. Technol., A **3**, 561–566 (1985).

[16]D. W. Hoffman, "Perspective on stresses in magnetron-sputtered thin films," J. Vac. Sci. Technol., A **12**, 953–961 (1994).

[17]J. A. Thornton, J. Tabock, and D. W. Hoffman, "Internal-stresses in metallic films deposited by cylindrical magnetron sputtering," Thin Solid Films **64**, 111–119 (1979).

[18]H. Windischmann, "Intrinsic stress in sputtered thin films," J. Vac. Sci. Technol., A **9**, 2431–2436 (1991).

[19]H. Windischmann, "Intrinsic stress in sputter-deposited thin films," Crit. Rev. Solid State Mater. Sci. **17**, 547–596 (1992).

[20]B. Window and N. Savvides, "Charged particle fluxes from planar magnetron sputtering sources," J. Vac. Sci. Technol., A **4**, 196–202 (1986).

[21]K. Eufinger, D. Poelman, H. Poelman, R. De Gryse, and G. B. Marin, "Effect of microstructure and crystallinity on the photocatalytic activity of TiO_2 thin films deposited by DC magnetron sputtering," J. Phys. D **40**, 5232–5238 (2007).

[22]K. Eufinger, D. Poelman, H. Poelman, R. De Gryse, and G. B. Marin, "Photocatalytic activity of DC magnetron sputter deposited amorphous TiO_2 thin films," Appl. Surf. Sci. **254**, 148–152 (2007).

[23]H. Poelman, K. Eufinger, D. Depla, D. Poelman, R. De Gryse, B. F. Sels, and G. B. Marin, "Magnetron sputter deposition for catalyst synthesis," Appl. Catal., A **325**, 213–219 (2007).

[24]S. Mahieu and D. Depla, "Reactive sputter deposition of tin layers: Modelling the growth by characterization of particle fluxes towards the substrate," J. Phys. D **42**, 053002 (2009).

[25]A. Barranco, A. Borras, A. R. Gonzalez-Elipe, and A. Palmero, "Perspectives on oblique angle deposition of thin films: From fundamentals to devices," Prog. Mater. Sci. **76**, 59–153 (2016).

[26]J. Erlebacher, M. J. Aziz, A. Karma, N. Dimitrov, and K. Sieradzki, "Evolution of nanoporosity in dealloying," Nature **410**, 450–453 (2001).

[27]Z. Lu, C. Li, J. H. Han, F. Zhang, P. Liu, H. Wang, Z. L. Wang, C. Cheng, L. H. Chen, A. Hirata, T. Fujita, J. Erlebacher, and M. W. Chen, "Three-dimensional bicontinuous nanoporous materials by vapor phase dealloying," Nat. Commun. **9**, 276 (2018).

[28]L. Maya, G. M. Brown, and T. Thundat, "Porous platinum electrodes derived from the reduction of sputtered platinum dioxide films," J. Appl. Electrochem. **29**, 881–888 (1999).

[29]F. Boydens, W. Leroy, R. Persoons, and D. Depla, "Deposition of thin films by sputtering cold isostatically pressed powder targets: A case study," Phys. Status Solidi A **209**, 524–530 (2012).

[30]P. Varga, T. Neidhart, M. Sporn, G. Libiseller, M. Schmid, F. Aumayr, and H. P. Winter, "Sputter yields of insulators bombarded with hyperthermal multiply charged ions," Phys. Scr. **T73**, 307–310 (1997).

[31]H. Rijckaert, G. Pollefeyt, M. Sieger, J. Hänisch, J. Bennewitz, K. D. Keukeleere, J. D. Roo, R. Hühne, M. Bäcker, P. Paturi, H. Huhtinen, M. Hemgesberg, and I. Van Driessche, "Optimizing nanocomposites through nanocrystal surface chemistry: Superconducting $YBa_2Cu_3O_7$ thin films via low-fluorine metal organic deposition and preformed metal oxide nanocrystals," Chem. Mater. **29**, 6104–6113 (2017).

[32]K. V. Aeken, S. Mahieu, and D. Depla, "The metal flux from a rotating cylindrical magnetron: A Monte Carlo simulation," J. Phys. D **41**, 205307 (2008).

[33]F. Boydens, W. Leroy, R. Persoons, and D. Depla, "The influence of target surface morphology on the deposition flux during direct-current magnetron sputtering," Thin Solid Films **531**, 32–41 (2013).

[34]J. E. Mayer and I. H. Wintner, "Measurements of low vapor pressures of alkali halides," J. Chem. Phys. **6**, 301–306 (1938).

[35]T. R. Wellman, "The vapor pleasure of NaCl over decomposing sodalite," Geochim. Cosmochim. Acta **33**, 1302–1303 (1969).

[36]J. W. Draper, "On the production of light by heat," Philos. Mag. J. Sci. **30**, 345–360 (1847).

[37]Z. Y. Chen, S. Zakipour, D. Persson, and C. Leygraf, "Effect of sodium chloride particles on the atmospheric corrosion of pure copper," Corrosion **60**, 479–491 (2004).